Ultraviolet Surface Plasmon-Coupled Emission Using Thin Aluminum Films

Ignacy Gryczynski, **Joanna Malicka**, **Zygmunt Gryczynski**, **Kazimierz Nowaczyk**, and **Joseph R. Lakowicz**[*]

Center for Fluorescence Spectroscopy, School of Medicine, Department of Biochemistry & Molecular Biology, University of Maryland, 725 West Lombard Street, Baltimore, Maryland 21201

Abstract

Surface plasmon-coupled emission (SPCE) is the directional radiation of light into a substrate due to excited fluorophores above a thin metal film. To date, SPCE has only been observed with visible wavelengths using silver or gold films. We now show that SPCE can be observed in the ultraviolet region of the spectrum using thin (20 nm) aluminum films. We observed directional emission in a quartz substrate from the DNA base analogue 2-aminopurine (2-AP). The SPCE radiation occurs within a narrow angle at 59° from the normal to the hemicylindrical prism. The excitation conditions precluded the creation of surface plasmons by the incident light. The directional emission at 59° is almost completely p-polarized, consistent with its origin from surface plasmons due to coupling of excited 2-AP with the aluminum. The emission spectra and lifetimes of the SPCE are those characteristic of 2-AP. Different emission wavelengths radiate at slightly different angles on the prism providing intrinsic spectral resolution from the aluminum film. These results indicate that SPCE can be used with numerous UV-absorbing fluorophores, suggesting biochemical applications with simultaneous surface plasmon resonance and SPCE binding assays.

Surface plasmon resonance (SPR) is widely used for detection of bioaffinity reactions on surfaces.[1–3] Surface plasmons are oscillating electrical charges on a metallic surface. When a thin metal film is illuminated through a glass prism, and the angle of incidence is appropriate, the surface plasmons in resonance with the incident light occur at the metal–air or water interface. This results in strong absorption, which is measured as a decrease of reflectivity. The SPR angle is sensitive to the refractive index of the sample above the metal, distal from the glass prism. The origin of this sensitivity is the evanescent field from the plasmons, which penetrates approximately $\lambda/3$ into the sample.

In several recent reports we described a related phenomenon, surface plasmon-coupled emission (SPCE).[4,5] We found that excited fluorophores near a thin metal surface can couple with the surface plasmons, resulting in directional radiation into the glass substrate. The spectral properties of the radiation were found to be essentially identical to those of the fluorophore, except for a highly p-polarized emission, too large to be due to optical photoselection. The angular dependence of the radiation, as well as the p-polarization, are consistent with radiating surface plasmons, the reverse process of surface plasmon absorption.

Our previous studies of SPCE used thin silver[5–7] or gold[8] surfaces. This choice of metals restricts the selection of fluorophores to those absorbing and emitting at visible or longer wavelengths. However, many widely used fluorophores absorb or emit at ultraviolet wavelengths. We now report that SPCE at UV wavelengths can be observed using thin

*To whom correspondence should be addressed: lakowicz@cfs.umbi.umd.edu.

aluminum films, enabling the use of SPCE with a wide variety of fluorophores and surface affinity reactions.

MATERIALS AND METHODS

Sample Preparation

Quartz slides were coated by vapor deposition by EMF Corp. (Ithaca, NY). A 20-nm-thick layer of aluminum was deposited on the quartz followed by a 10-nm SiO$_2$ protective layer (Scheme 1). Fluorophores were deposited on the surface by spin coating at 3000 rpm 1% solution of low molecular weight poly(vinyl alcohol) (PVA, MW. 13 000–23 000; Aldrich) in water. The PVA solutions contained 2-aminopurine (2-AP; 1.2×10^{-3} M) from Aldrich. The reference slide for the control experiment was prepared from identical 1% PVA solution without 2-aminopurine.

Reflectance Calculations

The reflectance profiles of the thin film were calculated with TFCalc. 3.5 software (Software Spectra, Inc., Portland, OR). The thicknesses of the samples were estimated by comparing the measured SPCE with the calculated reflectance for the emission wavelength.

Fluorescence Measurements

The spin-coated slides were attached to a hemicylindrical prism made of quartz using non-fluorescent index matching fluid (mixture of propylene glycol $n = 1.43$ and acetophenone $n = 1.53$). This combined sample was positioned on a precise rotary stage, which allows excitation and observation at any desired angle relative to the vertical axis around the cylinder.[5] For excitation we used the reverse Kretschmann (RK) configuration (Scheme 1). In this configuration, the sample was excited from the air or sample side, which has a refractive index lower than the prism. In this case, it is not possible to excite surface plasmons with the incident light. The angle of incidence does not matter, but we used normal incidence.

Observation of the angular distribution of the emission was performed with a 3-mm-diameter UV-transmitting fiber, covered with a 500-μm vertical slit, positioned ~15 cm from the sample. This corresponds to an acceptance angle below 0.2°. The output of fiber was directed to 8000 SLM spectrofluorometer or 10-GHz frequency domain fluorometer.[9]

For excitation, we used the second harmonic (300 nm) from a Rhodamine 6G dye laser. Dye laser was pumped by a mode-locked argon ion laser, 76-MHz repetition rate, 120-ps half-width, and cavity dumped at 3.8-MHz repetition rate. Scattered light at 300 nm was suppressed by observation through a cutoff 320-nm-long wave pass filter supported for intensity and lifetime measurements with a 370-nm interference filter.

The multifrequency phase and modulation data were analyzed in terms of the multiexponential model

$$I(t) = \sum_i \alpha_i \exp\left(-t/\tau_i\right)$$

(1)

where τ_i are the lifetimes with amplitudes α_i and $\Sigma\alpha_i = 1.0$. The parameters α_i and τ_i were determined by nonlinear least squares, as described previously.[10] The multiexponential model is used to describe the form of the intensity decay. We are not assigning molecular significance to the recovered parameters. The contribution of each component to the steady-state intensity is given by

$$f_i = \alpha_i \tau_i / \sum_j \alpha_j \tau_j$$

(2)

The mean decay time is given by

$$\bar{\tau} = \sum_i f_i \tau_i$$

(3)

The amplitude-weighted lifetime is given by

$$\langle \tau \rangle = \sum_i \alpha_i \tau_i$$

(4)

THEORY

SPCE is closely related to SPR. The angular distribution of the radiated light in the prism is determined by the same wavevector matching conditions as for SPR. For this reason, the theory for SPR can be used to describe the angular distribution of SPCE. The physics of surface plasmons has been described in detail.[11–13] Surface plasmons are excited when a metal surface is illuminated under specific conditions that allow wavevector matching at the sample–metal interface. Surface plasmons cannot be excited from air by incident light. SPR occurs when light is incident on a metal through a higher refractive index medium such as glass. The surface plasmons are only excited at a specific angle of incident (θ_{SP}) where the reflectivity decreases. At other angles of incidence (θ_I), the reflectivity of the metal is high.

The wavevector of the incident light in the prism is given by $k_p = 2\pi/\lambda = n_p k_0$, where λ is the wavelength in the prism, n_p is the refractive index of the prism, and k_0 is the wavevector in a vacuum or air. The in-plane x-component of the wavevector is given by

$$k_x = k_0 n_p \sin\theta_I$$

(5)

where θ_I is measured from the normal axis. SPR occurs when

$$k_{SP} = k_s = k_0 n_p \sin\theta_{SP}$$

(6)

where k_{SP} is the wavevector for the surface plasmons at the metal–sample interface. Calculation of the surface plasmon wavevector is somewhat complex. For a metal, the dielectric constant is usually an imaginary number

$$\varepsilon_m = \varepsilon_r + i\varepsilon_{im}$$

(7)

where $i = -1^{1/2}$ and the subscripts indicate the real (r) and imaginary (im) components. These constants are wavelength (frequency) dependent. Because the real part of ε_m is larger than the imaginary part, the surface plasmon wavevector can usually be approximated by

$$k_{SP} = k_0 \left(\frac{\varepsilon_r \varepsilon_s}{\varepsilon_r + \varepsilon_s} \right)^{1/2}$$

(8)

where ε_s is the effective dielectric constant of the sample near the silver surface. SPR only occurs for p-polarized incident light.

SPCE is similar to SPR in reverse. Instead of illumination through a prism, the metal film feels near-field interactions with an excited fluorophore, resulting in creation of surface plasmons. These plasmons then radiate into the glass substrate at the surface plasmon angle for the emission wavelength (θ_F in Scheme 1). The plasmons radiate at the plasmon angle because this is needed to match the wavevectors. The plasmons cannot radiate into the sample because the wavevectors cannot be matched. The angle θ_{SP} depends on wavelength because k_x and the optical properties of the metal depend on wavelength. Free-space (FS) emission of the fluorophore can also occur.

The dependence of SPR on the refractive index of the sample is due to the evanescent field from the plasmons which penetrates into the sample and decays exponentially away from the metal surface.[14] Based on the analogy between SPR and SPCE, we expect fluorophore coupling to the metal to also depend on the depth of the evanescent field. For SPR, the electrical field decays exponentially as

$$E_{SP}(z) = E_0 \exp(-k_z z)$$

(9)

where E_0 is the field strength at $z = 0$ and k_z^{-1} is the penetration depth into the sample. The values of k_z can be calculated using

$$k_z^2 = k_{SP}^2 - \varepsilon_s (\omega/c)^2$$

(10)

where ω is the frequency of the incident light.

RESULTS

As shown in previous reports,[4–7] the occurrence and angular distribution of SPCE can be predicted from the reflectivity curves of the thin silver and gold films. Knowing of the widespread use of UV fluorophores, we considered the use of different films of different metals. Aluminum was an obvious choice given the high reflectivity of aluminum mirrors at short wavelengths. An additional advantage of aluminum is that on exposure to air it forms a thin oxide film with a uniform self-limiting thickness. In our case, the aluminum film was coated with SiO_2. The use of aluminum with fluorescence was not obvious because of earlier reports of strong quenching on aluminum surfaces.[15] However, several reports described the transmission of ultraviolet light by thin aluminum films as seen by excitation of fluorescence with total internal reflection,[16] attenuated total internal reflection,[17] or light scattering.[18] Additionally, aluminum has been suggested for use in SPR,[19] and calculations of the spatial

distribution have been reported for fluorophores near an aluminum surface.[20] However, we are not aware of any experimental reports of SPR or SPCE using aluminum films.

Based on the absence of UV absorption by aluminum, we decided to calculate the reflectivity curves for thin aluminum films on quartz. These calculations were performed using commercial software (TFCalc) or our own equivalent programs. Reflectivity curves are shown in Figure 1 for various thicknesses of aluminum. These curves were calculated using the dielectric constant for aluminum at 370 nm. These results show that the deepest reflectivity minimum is for an aluminum thickness of 20 nm, which is the thickness we chose for our coated slides.

We were aware of aluminum oxidation, which can change an effective thickness of the metal layer. In the vapor deposition procedure, the slides were protected with a 100-Å SiO_2 layer, twice as thick as we used previously for silver mirrors.[5–7] The second reason for using thicker protection layer is to avoid the well-known quenching effect of aluminum.[15,20,21]

Because of earlier reports of quenching on aluminum surfaces, we first examined the free-space emission of spin-coated samples on quartz and an aluminum-coated quartz (Figure 2). Emission spectra were recorded for illumination and observation from the same side of the sample. Hence, plasmons were not created by the incident light and the emission of 2-AP was the free-space (FC) emission mostly uninfluenced by the metal. The emission spectrum of the spin-coated sample on quartz or aluminum was essentially the same as the spectrum observed for 2-AP in water in a square cuvette. This result is not in conflict with the reports of quenching on aluminum because our sample was distal from the metal surface by 100 Å and SPCE is thought to occur for distances up to 200 nm. Quenching probably occurs at shorter distances. The background emission from a reference slide without 2-AP (Figure 2, dotted line) is significantly lower than the observed 2-AP emission.

The presence of a sharp reflectivity minimum for 20-nm aluminum (Figure 1) suggested the presence of SPCE at the plasmon angle for the emission wavelength. The angle-dependent intensities are shown in Figure 3. The emission was found to be sharply distributed around ±59° from the normal axis. We were unable to measure the intensities for all angles on the sample side of the metal, but it appears that roughly 30% of the total emission from 2-AP appears as SPCE. This percentage does not represent the maximum coupling efficiency but is the result found with our particular thicknesses of aluminum, SiO_2, and PVA.

Next, we stored the samples in a dry environment at room temperature and measured SPCE once again next day. The measurement was highly reproducible in both angular distribution and intensity. Later, we washed out the PVA from the slide and spin-coated once again with 1% PVA solution doped with 2-AP as described in Materials and Methods. We repeated the SPCE measurements, and we were pleasantly surprised that the aluminum-coated slide with SiO_2 protection can be reused. We were not able to reuse the silvered slides with 50-Å SiO_2 protection. We concluded that there is no significant damage to the aluminum layer when protected with 100-Å SiO_2 coating.

Emission spectra of the SPCE are shown in Figure 4. Emission was only observed when the emission polarizer was in the p-orientation, meaning parallel to the plane of observation. The signal was over 20-fold less for an s-oriented polarizer. The high p-polarization of the signal proves its origin with surface plasmons and not free-space emission of 2-AP.

Examination of Scheme 1 shows that there is symmetry about the axis normal to the metal surface. There is no reason for the SPCE to occur in a plane, but rather should appear as a cone with equal intensities at all azimuthal angles around the normal axis. Because of the large angle θ_F it is difficult to capture the emission from the entire cone. We were able to capture and image the SPCE using a parabolic reflector (Figure 5). The cone of emission collected using

the parabolic reflectance is seen in the lower panel. The angular distribution appears to be narrow, but this is in part due to the reflector, which is focusing this distribution. These images show that a relatively simple optical configurations can be used to capture a large fraction of the total emission.

While we observed directional emission from 2-AP on aluminum, the 59° maximum angle was ~16° larger than that calculated for 20-nm aluminum on glass, which was ~43° (Figure 1). This difference is a result of the presence of two dielectric layers, a protective 10 nm of SiO_2 and the PVA doped with 2-AP. Hence, we repeated the reflectivity calculations using the five-phase system shown in Scheme 1, with an assumed PVA thickness of $d_s = 26.3$ nm. In this case, the reflectivity minimum for p-polarized incident light was at 59° (Figure 6), in precise agreement with the observed value. An s-polarized incident light did not show a calculated reflectivity minimum.

It is known that the angle of minimum reflectivity of silver and gold films depends on the incident wavelength.[22] As a result, different wavelengths radiate at slightly different angles in the prism.[5] Figure 7 shows the free-space emission spectra of 2-AP (top) and the emission spectra for different observation angles in the prism (bottom). The spectra are blue shifted at larger angles (62°) and red shifted at smaller angles (56°) compared to the central angle of 59°. This shift is not due to different local environments of 2-AP but rather to the intrinsic wavelength dispersion of SPCE.

In earlier studies of fluorophores near metallic particles,[23,24] we found decreases in lifetimes as compared to fluorophores distant from the particles. Hence, we examined the lifetime for 2-AP (Figure 8). The amplitude-weighted lifetime for the free-space emission was found to be 0.53 ns (top). The amplitude-weighted lifetime for SPCE was found to be 0.43 ns (bottom). In both cases, the lifetimes were multiexponential (Table 1). Compared to the dramatic reduction in lifetime near metallic particles,[23,24] the effect of the aluminum film is minimal. At this time we do not fully understand how the surface plasmons and fluorophores interact to determine the SPCE intensity decay.

It is of interest to consider the range of distances over which fluorophores couple with surface plasmons. This distance is likely to be related to the depth of the surface plasmon evanescent field in the sample. Hence, we calculated the penetration depths for gold, silver, and aluminum for several wavelengths (Table 2). These calculations show similar penetration depth in water for all three metals. The penetration depths of the evanescent waves are similar in PVA. Additionally, the optical properties of aluminum suggest that SPR and SPCE can occur down to 280 nm. This result suggests that SPR and SPCE will be possible using the intrinsic tryptophan fluorescence from proteins.

DISCUSSION

The measurements reported in this article are in a good agreement with the existing theory of SPR and the angle θ_F of the directional SPCE can be reliably predicted. The aluminized slides protected with the 100-Å SiO_2 layer are surprisingly stable and can be reused after washing. The wavelength resolution demonstrated in Figure 7 can be potentially used in construction of miniaturized SPCE based spectrofluorometer.

The observation of ultraviolet SPCE with aluminum suggests numerous applications in biochemistry, biotechnology, and medical testing. UV fluorophores are routinely used to label proteins and membranes. Examples include diphenylhexatriene and its derivatives, pyrenes, dansyl, and anilinonaphthalene-type fluorophores. Based on the results using 2-AP, such fluorophores should also display SPCE. Additionally, the optical properties of aluminum suggest SPCE will also be useful with intrinsic protein fluorescence.

Medical assays and biotechnology applications such as drug discovery frequently utilize surface-localized chemistry. Our results with aluminum indicate that the range of wavelengths can be extended down to the ultraviolet. This will provide a wide range of wavelengths for development of multianalyte assays using different color fluorophores. In summary, we believe SPCE will soon become a widely used technology in biomedical research and health care.

Acknowledgments

References

1. Salamon Z, Macleod HA, Tollin G. Biochim Biophys Acta 1997;1331:131–152. [PubMed: 9325439]

2. Melendez J, Carr R, Bartholomew DU, Kukanskis K, Elkind J, Yee S, Furlong C, Woodbury R. Sens Actuators, B 1996;35–36:212–216.

3. Liedberg B, Lundstrom I. Sens Actuators, B 1993;11:63–72.

4. Lakowicz JR. Anal Biochem 2004;324:153–169. [PubMed: 14690679]

5. Gryczynski I, Malicka J, Gryczynski Z, Lakowicz JR. Anal Biochem 2004;324:170–182. [PubMed: 14690680]

6. Matveeva E, Malicka J, Gryczynski I, Gryczynski Z, Lakowicz JR. Biochem Biophys Res Commun 2004;313:721–726. [PubMed: 14697250]

7. Lakowicz JR, Malicka J, Gryczynski I, Gryczynski Z. Biochem Biophys Res Commun 2003;307:435–439. [PubMed: 12893239]

8. Gryczynski I, Malicka J, Gryczynski Z, Lakowicz JR. J Phys Chem B. submitted for publication

9. Laczko G, Lakowicz JR, Gryczynski I, Gryczynski Z, Malak K. Rev Sci Instrum 1990;61:233–2337.

10. Lakowicz JR, Laczko G, Cherek H, Gratton E, Limkeman M. Biophys J 1984;46:463–477. [PubMed: 6498264]

11. Zayats AV, Smolyaninov II. J Opt A: Pure Appt Opt 2003;5:516–550.

12. Raether, H. Surface plasma oscillations and their applications. In: Hass, G.; Francombe, MH.; Hoffman, RW., editors. Physics of Thin Films, Advances in Research and Development. Vol. 9. Academic Press; New York: 1977. p. 145-261.

13. Raether, H. Surface Plasmons on Smooth and Rough Surfaces and on Gratings. Springer-Verlag; New York: 1988. p. 136

14. Hanken, DG.; Jordan, CE.; Frey, BL.; Corn, RM. Electroanalytical Chemistry: A Series of Advances. Vol. 20. Marcel Dekker; New York: 1998. Surface plasmon resonance measurements of ultrathin organic films at electrode surfaces; p. 141-225.

15. Weitz DA, Garoff S, Gersten JI, Nitzan A. J Chem Phys 1983;78(9):5324–5338.

16. Yokota H, Saito K, Yanagida T. Phys Rev Lett 1998;80(20):4606–4609.

17. Zerulla D, Isfort G, Kolbach M, Otto A, Schierbaum K. Electrochim Acta 2003;48:2943–2947.

18. Kume T, Hayashi S, Yamamoto K. Mater Sci, Eng 1996;A217/218:171–175.

19. de Bruijn HE, Kooyman RPH, Greve J. Appl Opt 1992;31(4):440–442.

20. Axelrod, D.; Hellen, EH.; Fulbright, RM. Total internal reflection fluorescence. In: Lakowicz, JR., editor. Topics in Fluorescence Spectroscopy: Biochemical Applications. Vol. 3. Plenum Press; New York: 1992. p. 289-343.

21. Ford, GW.; Weber, WH. Electromagnetic Interaction of Molecules with Metal Surfaces. Vol. 113. North-Holland Physics Publishing; Amsterdam: 1984. p. 195-287.

22. Natan, MJ.; Lyon, LA. Surface plasmon resonance biosensing with colloidal Au amplification. In: Feldheim, DL.; Foss, CA., Jr, editors. Metal Nanoparticles: Synthesis, Characterization, and Applications. Marcell Dekker; New York: 2002. p. 183-205.

23. Lakowicz JR, Shen Y, D'Auria S, Malicka J, Gryczynski Z, Gryczynski I. Anal Biochem 2002;301:261–277. [PubMed: 11814297]

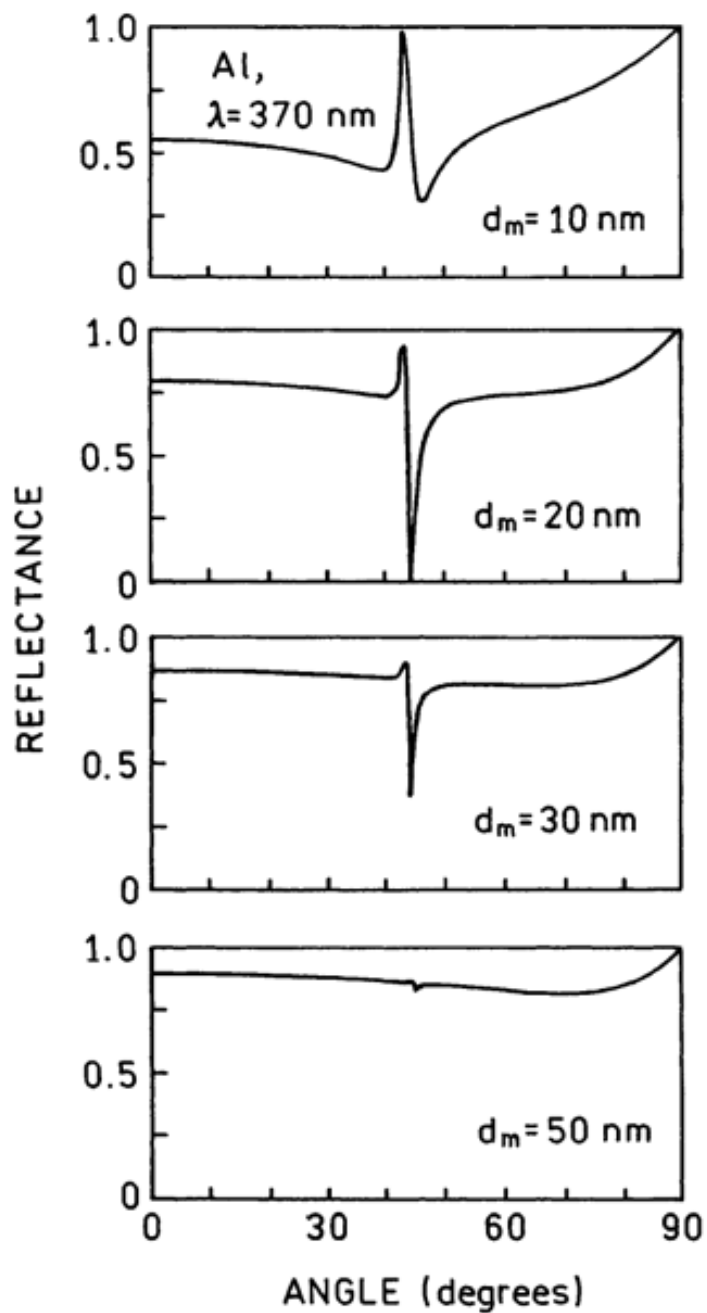24. Malicka J, Gryczynski I, Fang J, Lakowicz JR. Anal Biochem 2003;317:136–146. [PubMed: 12758251]

Figure 1.
Calculated reflectivity at 370 nm for a three-phase system of quartz–aluminum–air, for different thicknesses of aluminum. For 370 nm, we used $\varepsilon_m = -17.02 + i2.95$.
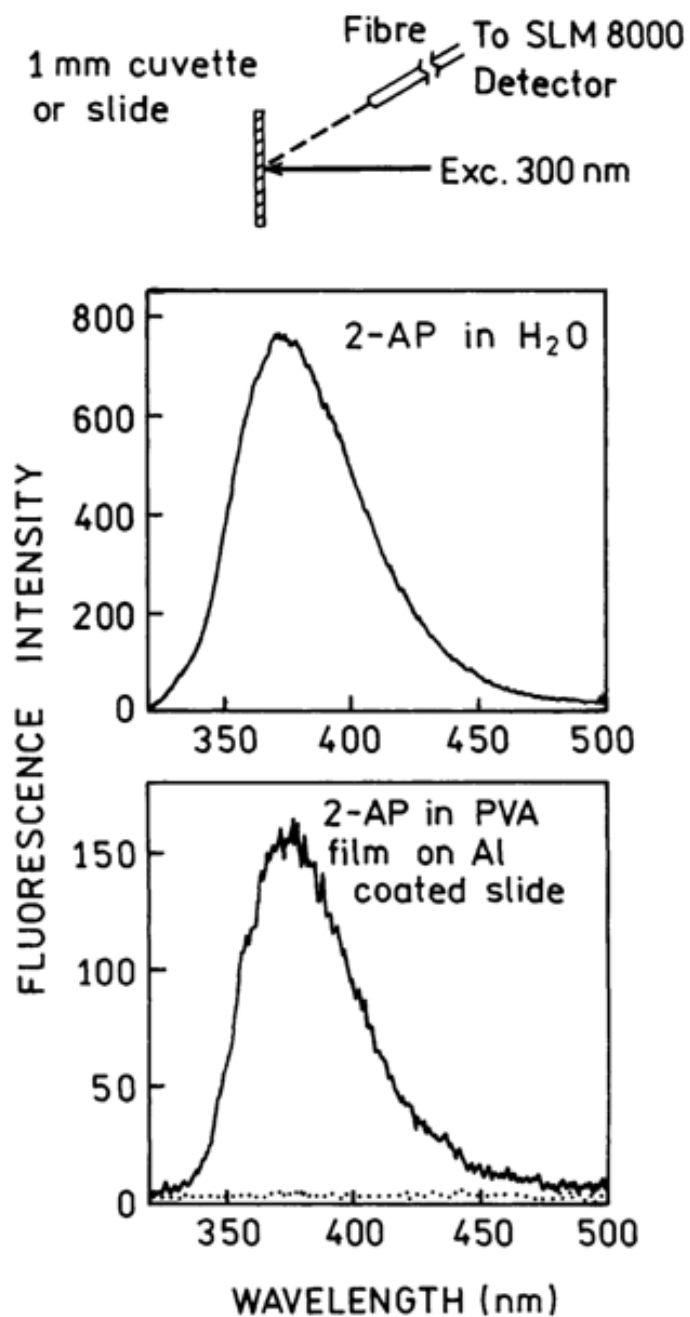
Figure 2.
Front face emission spectra of 2-AP in water (top) and spin-coated from 1% PVA on a 20-nm aluminum film (bottom). The spectrum of 2-AP in water (top) is identical to the spectrum measured in square geometry using a 1-cm square cuvette. The spectrum of 2-AP in PVA film on Al mirror is similar to the spectrum of 2-AP spin-coated from 1% PVA on unmetallized quartz slide. The dotted line is the background emission from the reference slide without 2-AP.
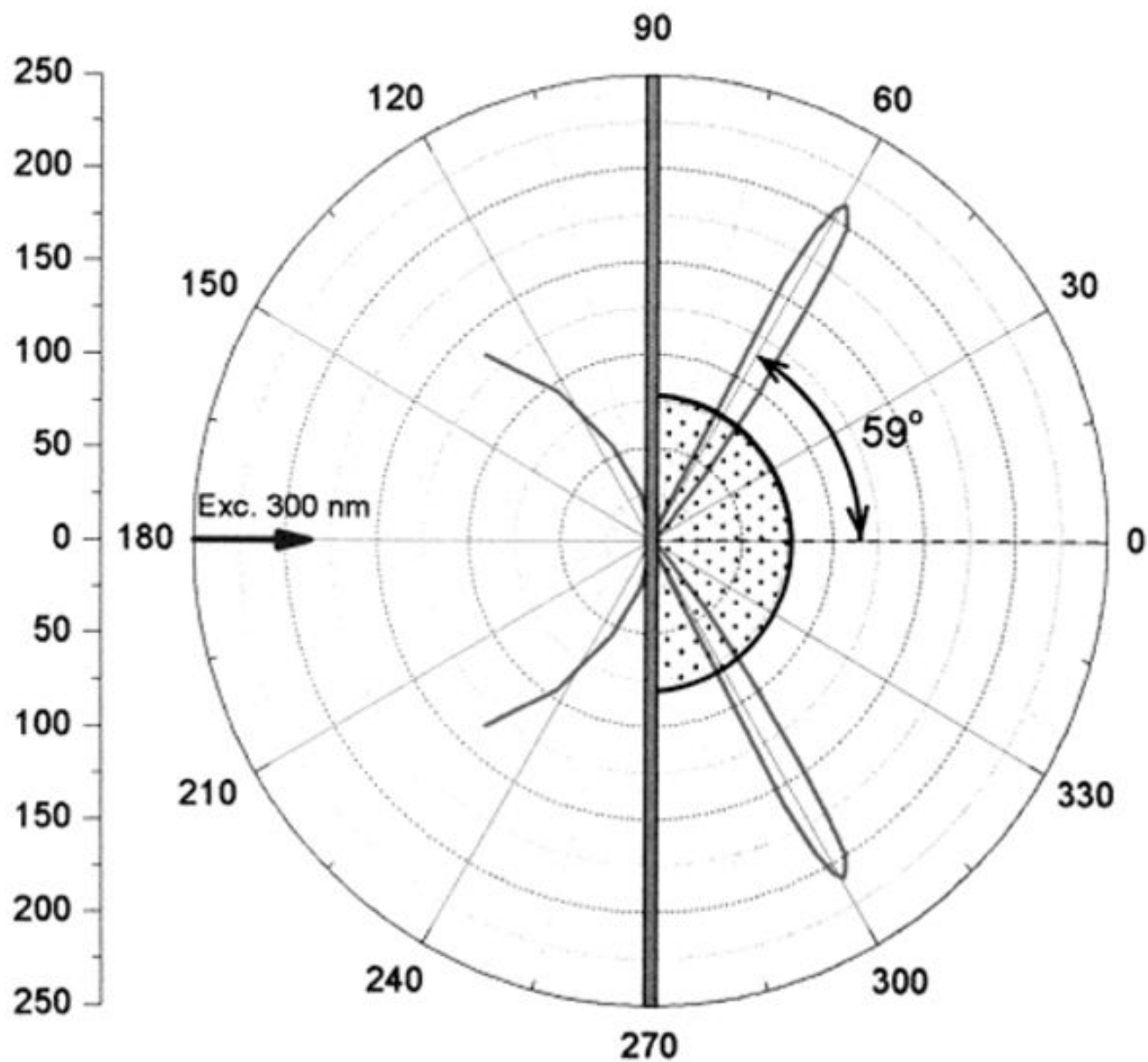
Figure 3.
Angle-dependent emission intensity of 2-AP at 370 nm with reverse Kretschmann excitation.
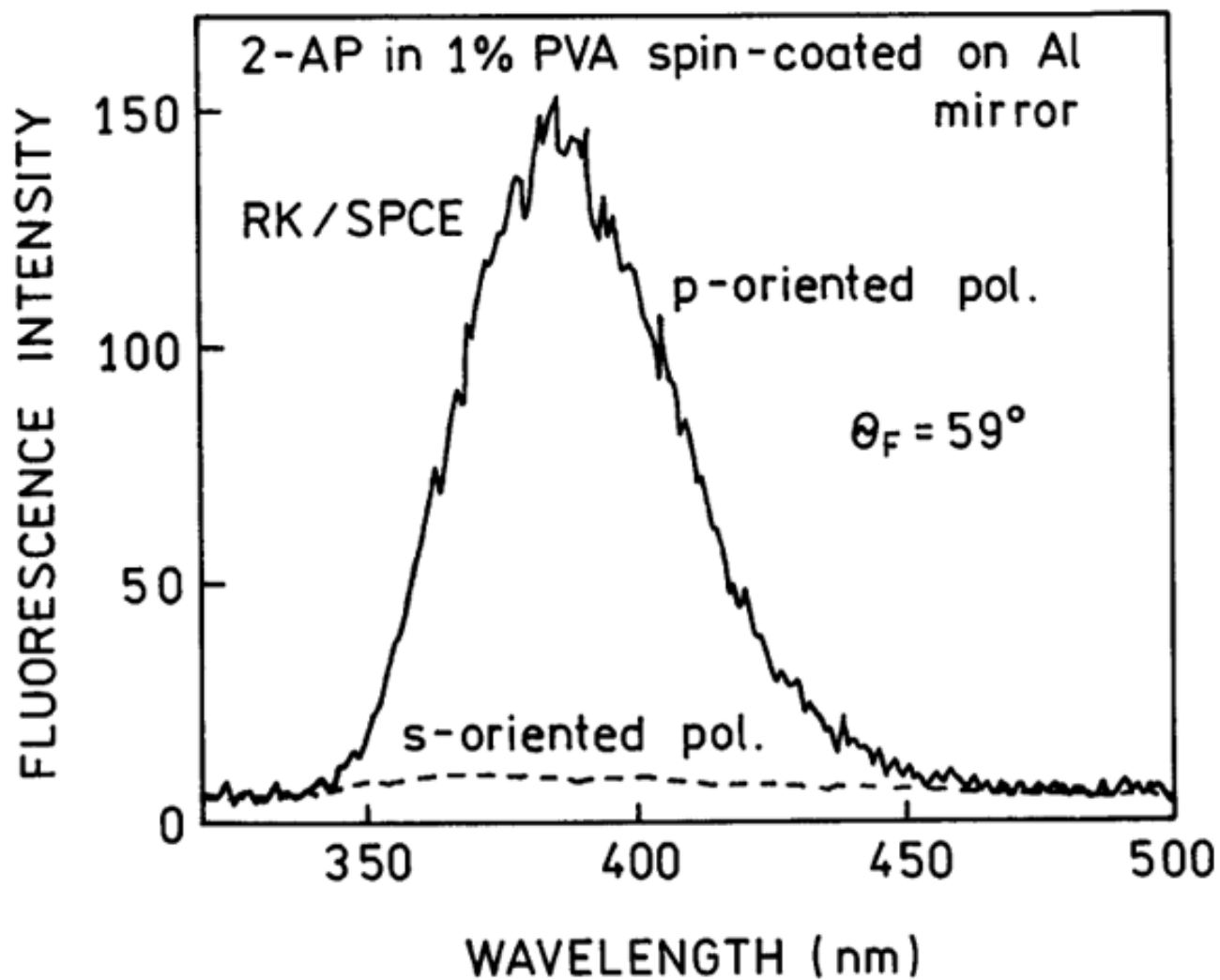
Figure 4.
Emission spectra of the SPCE from 2-AP with reverse Kretschmann excitation. The polarizer (pol.) orientation refers to the emission polarizer.
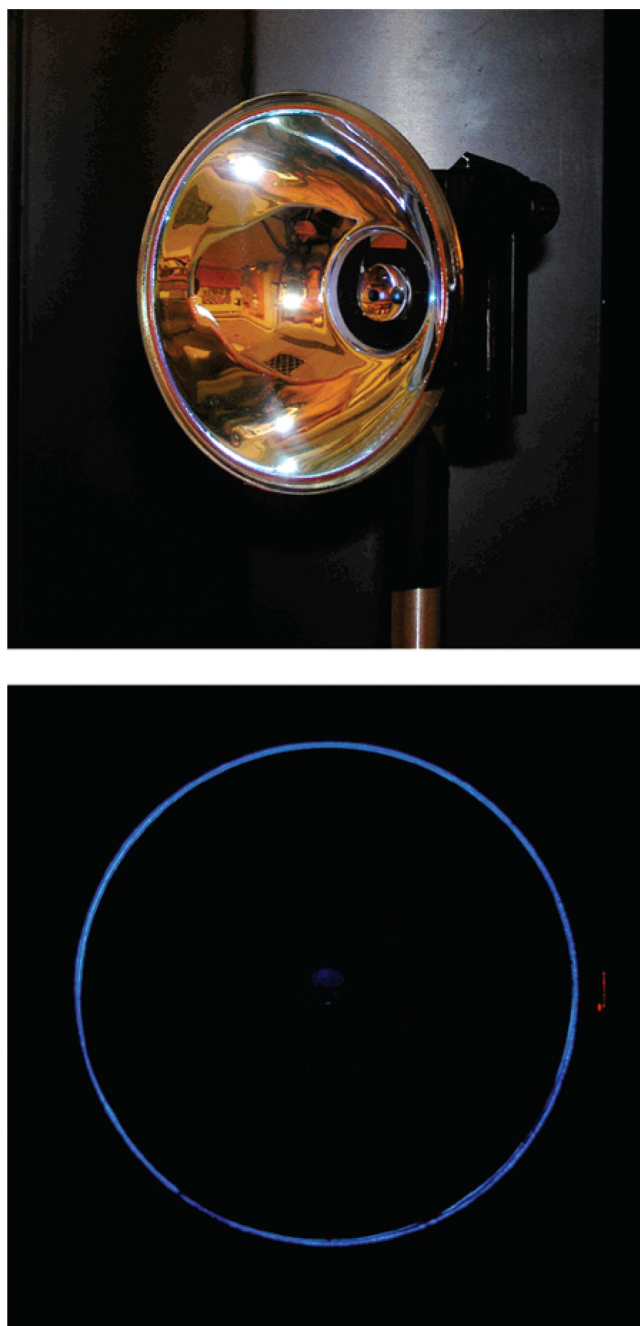
Figure 5.
Parabolic reflector used to capture SPCE (top) and the cone of emission for 2-AP observed using the reflector (bottom).
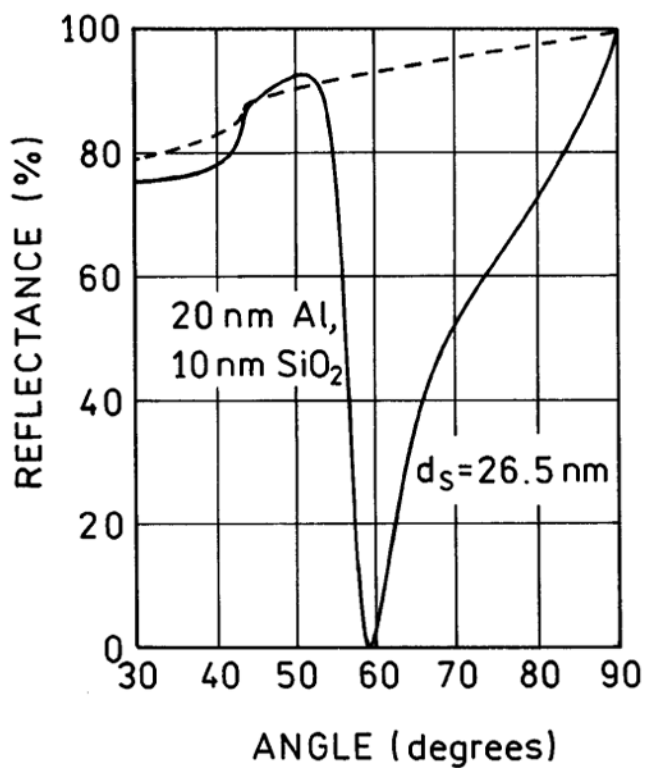
Figure 6.
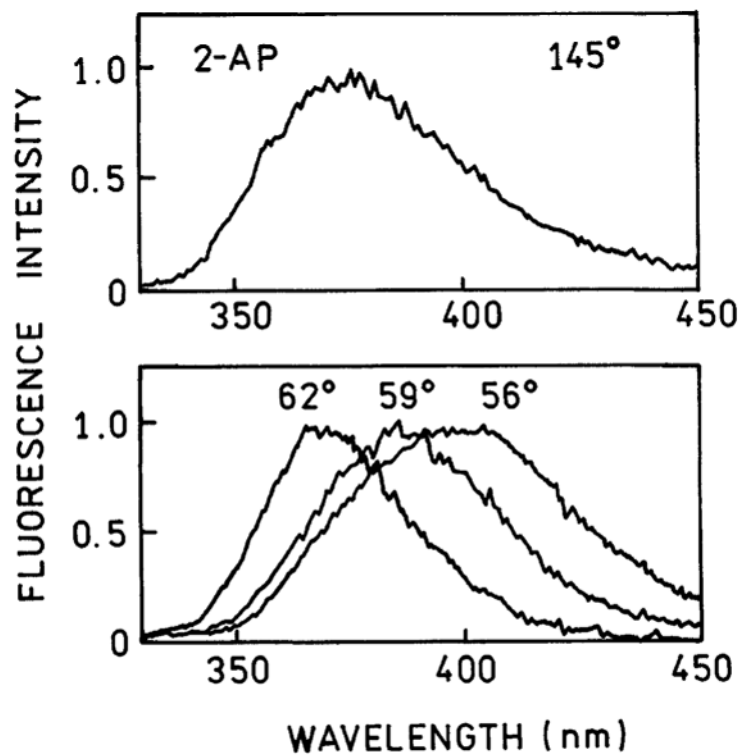Calculated reflectivity at 370 nm for the five-phase system shown in Scheme 1.

Figure 7.
Surface plasmon-coupled emission spectra of 2-AP recorded at different observation angles θ_F. The angles are defined on the figures.
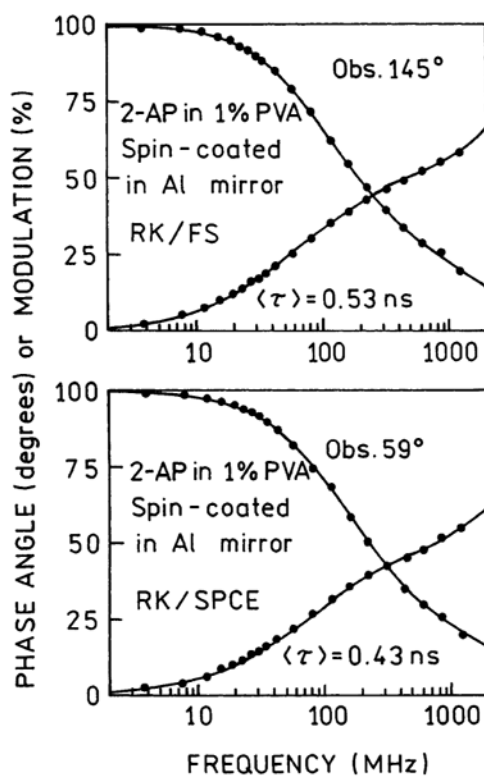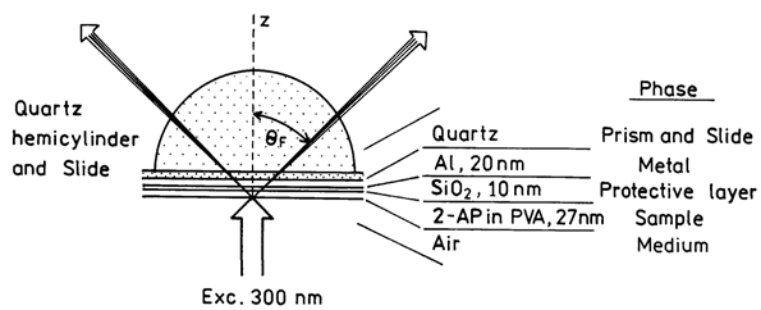
Figure 8.
Frequency-domain intensity decays of 2-AP with RK excitation. Top, FS. Bottom, SPCE.

Scheme 1.
Reverse Kretschmann Sample Configuration for SPCE Using a Thin Aluminum Film

Table 1

Multiexponential Intensity Decay Parameters for 2-AP in PVA on the Aluminum Film

measurement	a_i	f_i	τ_i (ns)	$\bar{\tau}$ (ns)	$\langle \tau \rangle$ (ns)
FS	0.69	0.15	0.12	1.84	0.53
	0.25	0.41	0.87		
	0.06	0.44	3.33		
SPCE	0.74	0.20	0.12	1.65	0.44
	0.22	0.47	0.93		
	0.04	0.33	3.60		

Table 2

Penetration Depth of the Surface Plasmon Evanescent Field into the Sample

metal	wavelength (nm)	$\varepsilon_m{}^a$	k_z^{-1} (nm) metal/water
gold	600	−8.37 + i 1.16	139
silver	600	−14.60 + i 0.45	193
aluminum	600	−42.30 + i 14.32	344
aluminum	370	−17.02 + i 2.95	131
aluminum	300	−11.03 + i 1.67	82
aluminum	280	−9.55 + i 1.37	70

[a] Interpolated values from TF Calc.